JGR Atmospheres

RESEARCH ARTICLE
10.1029/2021JD035316

Modeling Large-Scale Heatwave by Incorporating Enhanced Urban Representation

Pratiman Patel[1,2], Sajad Jamshidi[3], Raghu Nadimpalli[4], Daniel G. Aliaga[2], Gerald Mills[5], Fei Chen[6], Matthias Demuzere[7], and Dev Niyogi[8,9]

[1]Interdisciplinary Programme in Climate Studies, Indian Institute of Technology Bombay, Mumbai, India, [2]Department of Computer Science, Purdue University, West Lafayette, IN, USA, [3]Department of Agronomy, Purdue University, West Lafayette, IN, USA, [4]India Meteorological Department, New Delhi, India, [5]School of Geography, University College Dublin, Dublin, Ireland, [6]National Center for Atmospheric Research (NCAR), Boulder, CO, USA, [7]Department of Geography, Urban Climatology Group, Ruhr-University Bochum (RUB), Bochum, Germany, [8]Department of Geological Sciences, Jackson School of Geosciences, University of Texas at Austin, Austin, TX, USA, [9]Department of Civil, Architectural, and Environmental Engineering, Cockrell School of Engineering, University of Texas at Austin, Austin, TX, USA

Abstract This study evaluates the impact of land surface models (LSMs) and urban heterogeneity [using local climate zones (LCZs)] on air temperature simulated by the Weather Research and Forecasting model (WRF) during a regional extreme event. We simulated the 2017 heatwave over Europe considering four scenarios, using WRF coupled with two LSMs (i.e., Noah and Noah-MP) with default land use/land cover (LULC) and with LCZs from the World Urban Database and Access Portal Tools (WUDAPT). The results showed that implementing the LCZs significantly improves the WRF simulations of the daily temperature regardless of the LSMs. Implementing the LCZs altered the surface energy balance partitioning in the simulations (i.e., the sensible heat flux was reduced and latent heat flux was increased) primarily due to a higher vegetation feedback in the LCZs. The changes in the surface flux translated into an increase in the simulated 2-m relative humidity and 10-m wind speed as well as changed air temperature within cities section and generated a temperature gradient that affected the temperatures beyond the urban regions. Despite these changes, the factor separation analysis indicated that the impact of LSM selection was more significant than the inclusion of LCZs. Interestingly, the lowest bias in temperature simulations was achieved when WRF was coupled with the Noah as the LSM and used WUDAPT as the LULC/urban representation.

Key Points:

- Sensitivity of weather research and forecasting model (WRF) heatwave simulation to surface parameterization and urban heterogeneity
- First results to show the use of local climate zones improves large-scale WRF simulation
- Urban representation can affect temperatures beyond the urban grids regionally

Supporting Information:

Supporting Information may be found in the online version of this article.

Correspondence to:

D. Niyogi,
happy1@utexas.edu

Citation:

Patel, P., Jamshidi, S., Nadimpalli, R., Aliaga, D. G., Mills, G., Chen, F., et al. (2022). Modeling large-scale heatwave by incorporating enhanced urban representation. *Journal of Geophysical Research: Atmospheres*, *127*, e2021JD035316. https://doi.org/10.1029/2021JD035316

Received 1 JUN 2021
Accepted 9 JAN 2022

Author Contributions:

Conceptualization: Pratiman Patel
Formal analysis: Pratiman Patel, Sajad Jamshidi, Dev Niyogi
Funding acquisition: Dev Niyogi
Investigation: Pratiman Patel, Sajad Jamshidi, Gerald Mills, Fei Chen, Dev Niyogi
Methodology: Pratiman Patel, Sajad Jamshidi, Raghu Nadimpalli
Software: Pratiman Patel, Sajad Jamshidi, Raghu Nadimpalli
Supervision: Dev Niyogi
Validation: Sajad Jamshidi, Raghu Nadimpalli
Visualization: Pratiman Patel, Sajad Jamshidi
Writing – original draft: Pratiman Patel, Sajad Jamshidi
Writing – review & editing: Pratiman Patel, Sajad Jamshidi, Raghu Nadimpalli, Gerald Mills, Fei Chen, Matthias Demuzere

1. Introduction

Human-induced climate change has resulted in a notable increase in extreme events. For the European region, it includes more intense and frequent heatwaves (IPCC, 2014), increase in heavy precipitation events (Nissen & Ulbrich, 2017), and snow cover reduction in Northern Europe (Croce et al., 2018). Also, it is projected that the winter temperature in Northern Europe and the summer temperature in Mediterranean regions may exceed the global warming rate of the previous century (IPCC, 2013). The vulnerability of European cities to higher temperatures continues to be highlighted with reports of large numbers of fatalities. For example, the 2003 heatwave event caused more than 70,000 fatalities across Europe (Robine et al., 2008), and from 1992 to 2017, heatwaves might have led to more than 37,500 fatalities in Germany alone (An der Heiden et al., 2020).

Urban dwellers are highly susceptible to heatwaves where the fatality risk increases by 4.5% for every 1°C increase in heatwave intensity (Anderson & Bell, 2010). The higher vulnerability is primarily due to the population's density, and the pre-existing Urban Heat Island effect, which produces higher temperature in urban areas than the underdeveloped surroundings (Oke, 1982). The warming in built-up areas has been attributed to the modified thermodynamic properties of artificial surfaces, reduction of wind speed due to the increased urban roughness, long-wave radiation trapping during night time, lack of green surfaces, and the anthropogenic heat generated by human activities (Mahmood et al., 2014; Schwarz & Manceur, 2015). The integration of climatic changes and urbanization makes the dynamics of heatwave events more complex. However, by enabling the models with better physics and data capabilities, simulating such events over the urban areas could be improved (Hertwig et al., 2020; Zhao et al., 2021).

The Weather Research and Forecasting (WRF) model is a community model widely used in numerical weather prediction and (regional) climate simulations (Powers et al., 2017). WRF has dynamically integrated land surface

models (LSMs) with urban canopy models (UCMs) to represent the physical processes and land surface fluxes in an urban environment. The Noah land surface model (Chen & Dudhia, 2001; Chen et al., 1996; Ek et al., 2003) represents the land surface elements using simplified bulk surface properties. A modification of the Noah-LSM model is the Noah-MP, which incorporates multiple parameterizations for a range of land-atmospheric interaction processes (Niu et al., 2011; Z. L. Yang et al., 2011). The WRF model (V4.1) employs three different urban models, namely, the single-layer UCM (Chen et al., 2011), multi-layer UCM [building environment parameterization (BEP); Martilli et al., 2002], and building energy model (BEM; Salamanca & Martilli, 2010) schemes.

The combination of different LSMs and UCMs provides different physics parameterization options that permit ensemble simulations. For example, simulations of the series of heatwave events in Australia showed that the default Noah-LSM had a better performance than Noah-MP (Imran et al., 2018), while the Noah-MP coupled with the BEP-BEM improved the root mean square error (RMSE) of the simulated air temperature estimates (in Beijing, China) by 0.9°C (32%) compared to the Noah-LSM (Xu et al., 2018). Thus, depending on the application of interest, geographical locations, and the problem's spatiotemporal scale, it is likely that the physics choice could vary and requires additional studies.

One of the requirements for UCMs is identifying data that represents the scales and applications being considered (Demuzere et al., 2017). In particular, the urban morphology may not be available for many cities, or the data quality may not meet the required spatiotemporal resolution (Salamanca et al., 2011). In recent years, efforts such as the World Urban Database Access Portal Tool (WUDAPT) have helped to generate a consistent urban database using local climate zone (LCZ) maps. The LCZ framework usually classifies the urban region into ten different urban classes based on the roughness and density of buildings, surface cover around the feature, and thermal properties of the materials (Ching et al., 2018; Stewart & Oke, 2012). Examples of studies incorporating LCZ information into WRF include simulations over Madrid, Spain (Brousse et al., 2016), Vienna, Austria (Hammerberg et al., 2018), Szeged, Hungary (Molnár et al., 2019), Mumbai, India (Patel et al., 2020), and Bologna, Italy (Zonato et al., 2020). These studies consistently report an improvement in the model skill to simulate air temperature, precipitation, and wind speed.

However, these studies are on a single city, while provide insights on urban-atmospheric processes within urban boundaries, may not account for the synergistic interactions between urban areas and the larger regional environments. Such interactions may have substantial implications in exploring how heatwave impacts urban areas (Li & Bou-Zeid, 2013). Therefore, it is important to understand the regional scale feedback of the urban environments on a synoptic scale event such as a heatwave. Also, the impacts of the heatwaves are worst over the urban areas, and in Europe approximately 75% of the total population lives in the urban environment (World Bank, 2021). Thus, it becomes necessary to simulate heatwaves and document the simulation uncertainties.

In this study, we advance the understanding of the impacts of large scale urban feedback on the 2017 European heatwave event. The simulations were carried out using WRF's Noah and Noah-MP LSMs and with and without LCZ information.

2. Methodology

2.1. 2017 June Europe Heatwave

June 2017 was remarkable in Europe as it was the starting point for exceptional hot weather that prevailed for the next 3 months (Hartfield et al., 2018). The heatwave started on 10 June and extended till 23 June, 2017, peaking between 16 and 18 June. The onset was from 10 to 15 June, and the decay period was 19–23 June. In Spain, it was documented as the hottest June since 1965, and in Switzerland and France, it was the second hottest June since 1864 and 1990, respectively. Local meteorological observatories reported extreme temperatures, such as, on 21 June, the Heathrow airport (UK) recorded 307.6 K (34.5°C), the warmest June day since 1976. The minimum night temperatures reached above 298.1 K (25°C) in Switzerland, leading to the warmest nights since 1981. The extreme temperature led to drought conditions across western Europe and contributed to substantial wildfires. Detailed information about the 2017 June heatwave event is provided in Sánchez-Benítez et al. (2018).

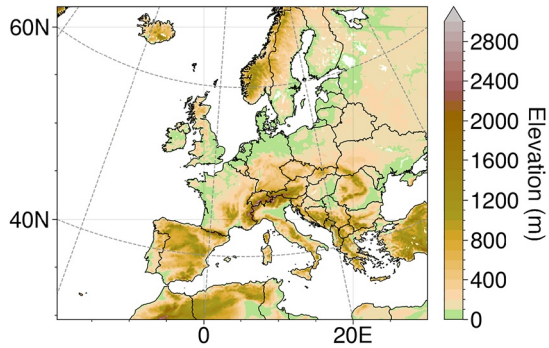

Figure 1. The Weather Research and Forecasting model (WRF) domain configuration over the study area (Europe) with topography (m). The WRF domain was configured in a 9 km grid spacing with the initial and boundary condition from National Centers for Environmental Prediction Final Operational Model, for the period of 8 June to 25 June.

2.2. Modeling Framework

The WRF model (version 4.1.4; Skamarock et al., 2019) is a non-hydrostatic primitive equation model that utilizes different physics parameterization options. The model domain was configured with a 9 km grid spacing (547 × 462 grid cells) with 51 vertical levels covering Europe (shown in Figure 1). The initial and boundary conditions are provided by National Centers for Environmental Prediction Final Operational Model Global Tropospheric Analyses (NCEP FNL) data (available at http://rda.ucar.edu/datasets/ds083.2), which is available at a 6-hr and 0.5° temporal and spatial resolution, respectively. The simulations started on 8 June 2017 00:00 UTC and ended on 25 June 2017 00:00 UTC. The following parameterization schemes were used in the study: the rapid radiative transfer model scheme (Mlawer et al., 1997) for longwave radiation, Goddard (Chou & Suarez, 1994) shortwave scheme, Bougeault-Lacarrère (Bougeault & Lacarrere, 1989) for the planetary boundary layer, WRF single moment six-class (Hong & Lim, 2006) scheme as microphysics, Kain-Fritsch (Kain, 2004) as cumulus scheme, and multi-layer BEP (Martilli et al., 2002) as the urban scheme, which is similar to the suggestions by Stergiou et al. (2017) and Politi et al. (2018). Anthropogenic heat flux (AHF) from building space heating and cooling is considered by setting a fixed temperature inside buildings in the BEP. AHF from other sources (e.g., human metabolism, vehicles, and power plants) are thereby neglected. The simulations are performed using two LSMs that is, Noah and Noah-MP.

For the land use/land cover (LULC), the Moderate Resolution Imaging Spectroradiometer (MODIS) data is used in two ways: (a) the default MODIS LULC which has one urban class "Urban and Built-up Lands" (Figure S1a in Supporting Information S1); and (b) the MODIS LULC product in which its original urban land cover is replaced by the 10 urban LCZ classes, available from the European LCZ map at 100 m spatial resolution (Demuzere et al., 2019a, 2019b; hereafter denoted as WUDAPT LULC; Figure S1b in Supporting Information S1). Given the MODIS LULC availability at 1 km spatial resolution, the LULC data for each urban grid was defined based on the majority class classified by WUDAPT within that grid.

An important objective of WUDAPT, WUDAPTs community project, is to generate urban canopy information and provide the (open-source) tools to facilitate urban-focused modeling studies (Ching et al., 2018). As such, WUDAPT's Level-0 information (the LCZ maps) can be converted to urban canopy parameters (UCP) that can be used in models (Ching et al., 2019). Since the work of Brousse et al. (2016), the level-0 WUDAPT information, the LCZ maps, have been used in WRF. The WUDAPT-to-WRF tool (Martilli et al., 2016) is publicly available, and assigns the corresponding morphological, radiative, and thermal UCPs to the LCZ class corresponding to each WRF grid cell. However, Zonato et al. (2020) recently argued that it is better to assign morphological parameters directly to the high-resolution LCZ grid, afterward aggregated to the lower-resolution WRF grid. The method consequently produces a unique urban morphology parameter value for each WRF grid cell, found to be more efficient in reproducing urban boundary layer features especially in the outskirts of cities and is in line with the WUDAPT-to-COSMO routine developed by Varentsov et al. (2020). Since an updated version of the WUDAPT-to-WRF tool is currently still being developed, the default approach by Brousse et al. (2016) and Martilli et al. (2016) is used here where the LULC is resampled from 1 to 9 km resolution based on the majority class or dominant category. For example, if a 9 km resolution grid consist of three classes LCZ 1 (30%), LCZ 2 (30%), and LCZ 3 (40%), then LCZ 3 will be assigned to that grid. This method is commonly used (default) in the WRF modeling (use dominant category only). If the urban or LCZ coverage is less than 50% but dominant than the urban or LCZ will be used, with the urban fraction same as the urban or LCZ. The urban parameters used in the study are shown in Table S1 in Supporting Information S1.

After resampling the WUDAPT map, the following LCZs (percentage urban cover with respect to total LCZ area) were available for analysis: LCZ 2 (compact mid-rise; 1%), LCZ 5 (open mid-rise; 2%), LCZ 6 (open low-rise; 76%), LCZ 8 (large low-rise; 10%), and LCZ 9 (sparsely built; 11%). All other urban LCZs were unavailable at the spatial resolution of 9 km. Examples of the differences between the urban area representation in the MODIS and WUDAPT are shown in Figure 2. It can be noted that a few pixels in WUDAPT are represented by MODIS urban class due to the WRF pre-processing system.

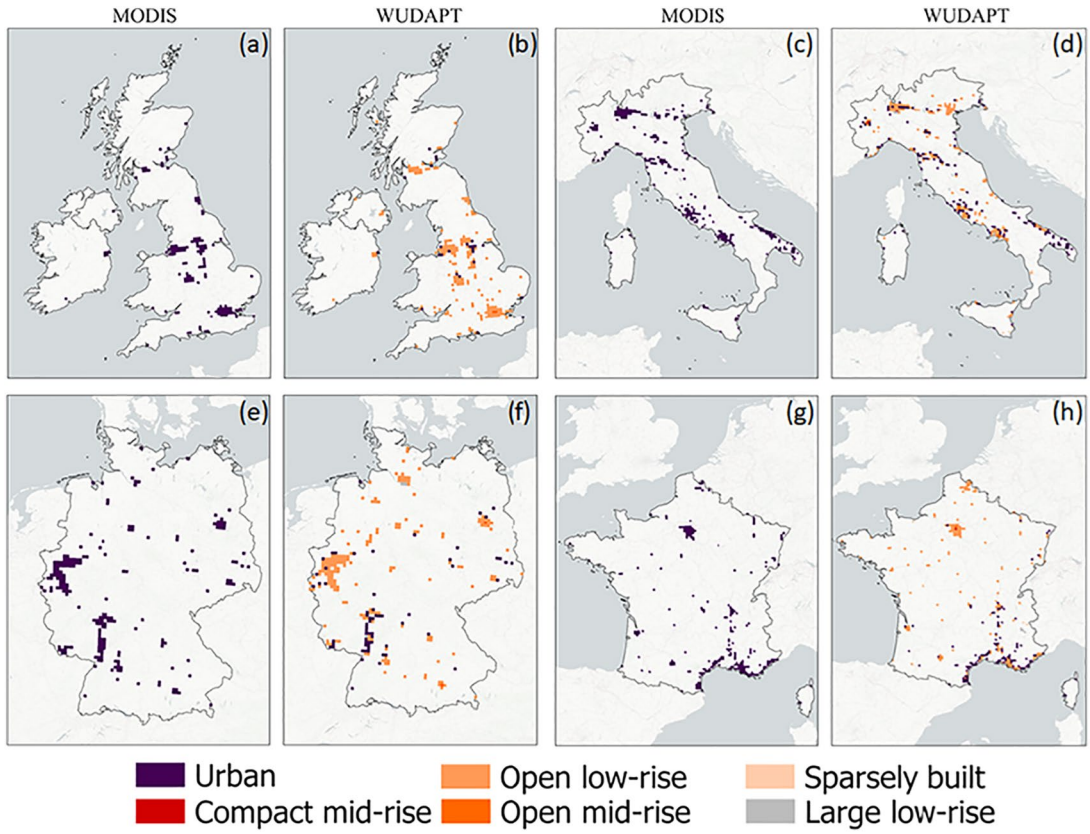

Figure 2. Examples of urban areas representation in the Moderate Resolution Imaging Spectroradiometer and World Urban Database and Access Portal Tool land use/land cover maps for the United Kingdom (a, b), Italy (c, d), Germany (e, f), and France (g, h).

Noah LSM has been developed based on multi-institutional cooperation (Chen et al., 1996; Ek et al., 2003) and considers the land surface as a blend of surface elements defined by the bulk properties. Despite its vast applications in operational weather and climate predictions, the Noah model is known to have biases in simulating surface features and fluxes (Slater et al., 2007). Therefore, Niu et al. (2011) augmented the representations of land surface processes in Noah by implementing multiple parameterization schemes (named as Noah-MP). Noah and Noah-MP differ in the conceptualization of five major processes including energy balance in vegetation canopy, vegetation phenology, soil infiltration, snowpack, and the interaction between groundwater soil moisture and runoff.

Noah considers an implicit vegetation-soil surface to drive surface energy components. A single layer energy-mass balance for snow simulations and the absence of groundwater transfer and storage impedes Noah ability to accurately account for heat and energy exchange between soil-vegetation-atmosphere continuum. In Noah-MP, a separate vegetation canopy layer has been implemented that enables the model to simulate the radiation transmitted and attenuated through and below canopy. Noah-MP also considers different biophysical options for transpiration, a dynamic vegetation model, a multi-layer snow energy–mass balance model, surface water infiltration, and groundwater processes.

2.3. Numerical Experiments

A 2 × 2 experimental setup was designed with the WRF domain covering the 2017 Europe heatwave (8–25 June). Two experiments were performed using the Noah model: one used the default MODIS LULC (denoted as N), and the second used the WUDAPT LULC (denoted as the N-W). Other two experiments were performed with the Noah-MP LSM: one used the default MODIS LULC (denoted as N-MP), and one used the WUDAPT LULC (denoted as the N-MP-W). The combination of two LSMs options (Noah and Noah-MP) without and with urban

heterogeneity (MODIS and WUDAPT, respectively) were evaluated for their performance to simulate the heatwave event. All other physics and inputs remained the same for all the simulations, as noted above.

2.4. Observations and Model Evaluation

Daily mean (T_{mean}), maximum (T_{max}), and minimum temperature (T_{min}) were retrieved from the E-OBS temperature data set (v 22.0 e; Cornes et al., 2018) and used to evaluate the model output. E-OBS provides quality-controlled gridded data at the spatial resolution of 0.1 degrees (daily) from more than 4,000 stations spread all over Europe. The observations have been validated and used as reference measurements in various meteorological studies conducted over Europe (Krauskopf & Huth, 2020; Lorenz et al., 2019). Due to a relatively sparse network of stations, Kyselỳ and Plavcová (2010) have reported on the interpolation uncertainty of the old versions of E-OBS products, which was resolved with the denser network across Europe and using the ensemble version (Cornes et al., 2018) as we used in our study.

We highlight that the *in situ* network's density used in developing the gridded E-OBS data may not adequately capture and represent the urban heterogeneity. Also, the density across different LCZs for the study domain is unclear and should be undertaken as done, for instance, by Montandon et al., 2011 for different landscape types represented in the Global Historical Climate Network. However, given that no other homogeneous high-resolution gridded air temperature datasets were available that do properly account for urban regions, and the fact that the E-OBS data and the WRF runs are of similar spatial scale (the E-OBS data set is prepared at 0.1° similar to the 9 km grid spacing in the WRF simulations), we assume that spatial aggregation of the area represented within the grids will be comparable with each other.

The simulated 2-m air temperature (within the urban canopy layer), which matches the setup of the observation stations, was evaluated against the observations using the unbiased RMSE (uRMSE) as given by the following equation:

$$uRMSE = \sqrt{\left[\frac{1}{n}\sum_{i=1}^{n}(f_i - o_i)^2\right]^2 - \left[\frac{1}{n}\sum_{i=1}^{n}(f_i - o_i)\right]^2} \quad (1)$$

where f_i is the forecast value, o_i is the observed value, and n is the total number of observations. The observed and simulated temperature were spatially averaged over the urban areas, and for each LCZ were compared using uRMSE and Taylors diagram (Taylor, 2001) for correlation coefficient, standard deviation, and RMSE. It facilitates the intercomparison of different model simulations. The resulting comparison helped in identifying the combination of LULC and LSM that generates the least error.

To understand the nonlinear interaction between the LSM and LULC, we used the factor separation method proposed by Stein and Alpert (1993). The following annotations are used for the influencing factors:

$$f_0 : \text{N, only Noah (both factors set to default)}$$

$$f_1 : \text{N-W, Noah with WUDAPT (LULC effect)}$$

$$f_2 : \text{N-MP, only Noah MP (LSM effect)}$$

$$f_{12} : \text{N-MP-W, Noah MP with WUDAPT (both LULC and LSM effect)}$$

The model results were analyzed for the direct and interactive effects as:

$$F1 = f_1 - f_0 \quad (2)$$

$$F2 = f_2 - f_0 \quad (3)$$

$$F12 = f_{12} + f_0 - f_1 - f_2 \quad (4)$$

where F1 is the direct LULC effect, F2 is the direct effect of the LSM, and F12 is the combined or interactive effect of LULC and LSM on the simulation of the event. We applied the factor separation analysis to quantify the relative importance of (a) the LULC, (b) the land surface parameterization, and (c) the combined effect of

LULC and land surface parameterization. Similar analysis have been carried out in Niyogi et al. (2006) and L. Yang et al. (2019) for separating the contribution of urban environment and topography to the spatial-temporal distribution of rainfall in urbanized regions.

The factor separation of the simulations was also calculated for the maximum heat index (HI) as a variable. The HI is a measure of the "thermal sensation" temperature for shaded locations that quantify the actual heat being experienced by individuals (Rothfusz & Headquarters, 1990). Thus, we used it to better represent the heatwave impact on human thermal comfort. In this study, HI was calculated using the standard procedure adopted by the U.S. National Weather Service formula (https://www.wpc.ncep.noaa.gov/html/heatindex_equation.shtml) that was originally proposed by Steadman (1979) and modified by Rothfusz and Headquarters (1990).

$$HI = -0.5[T + 61.0 + (T - 68.0)1.2 + (0.1RH)] - F_{adj} \tag{5}$$

For the environmental conditions that warrant a HI > 80 °F, the HI formula is replaced by Equation 6. Factor separation was computed using these equations of HI.

$$\begin{aligned} HI = \big[&-42.379 + 2.050T + 10.143RH - 0.225(T)(RH) - 0.007(T)^2 - 0.055 \times (RH)^2 \\ &+ 0.001(T)^2(RH) + 0.001(T)(RH)^2 - 1.99 \times 10^{-6}(T)^2(RH)^2\big] - F_{adj} \end{aligned} \tag{6}$$

where, T is the temperature in degrees F (°F), RH is the relative humidity (%), HI is the heat index expressed as an apparent temperature in °F (converted to °C), F_{adj} is an adjustment factor that is applied for certain humidity and air temperature conditions:

$$\begin{cases} RH < 13\%; 80 < T < 112°F \rightarrow F_{adj} = \dfrac{13 - RH}{4}\sqrt{\dfrac{17 - |T - 95|}{17}} \\ RH < 85\%; 80 < T < 87°F \rightarrow F_{adj} = \dfrac{RH - 85}{10} \times \dfrac{87 - T}{5} \\ \text{For all other conditions} \rightarrow F_{adj} = 0 \end{cases}$$

The Steadman method used in this study is one possible measure for thermal sensation and other methods such as physiological equivalent temperature or universal thermal climate index could be used for heat index assessments. However, we used this operational heat index as it provided a straightforward concept from decision-making standpoint where the error and uncertainty of model simulations in human comfort needs to be understood.

2.5. Surface Energy Balance

Positive feedback from irregular surface boundary conditions has been reported as an important criterion for generating and regulating drought and heatwaves (Miralles et al., 2014; Teuling et al., 2010). The foundation for such feedback involves the changes in the surface energy budget. Therefore, we analyzed the diurnal fluxes in the urban areas during the heatwave event by considering how the energy is partitioned in the different simulations. The surface energy balance provides insights to understand the regional heat budget and mechanisms that cause temperature changes among the experiments. The following equation gives the surface energy balance:

$$Q^* = Q_h + Q_e + Q_g \tag{7}$$

where Q^* is net radiation, Q_g is the ground heat flux, Q_e is the latent heat flux, and Q_h is the sensible heat flux. The ground heat flux refers to the energy transferred in the soil and is typically much smaller than the other fluxes. The net incoming solar radiation is balanced by the changes in sensible and latent heat transfers (neglecting the soil heat storage). Therefore, considering net radiation to be roughly stable, increases in sensible heat flux must be compensated by decreases in latent heat flux.

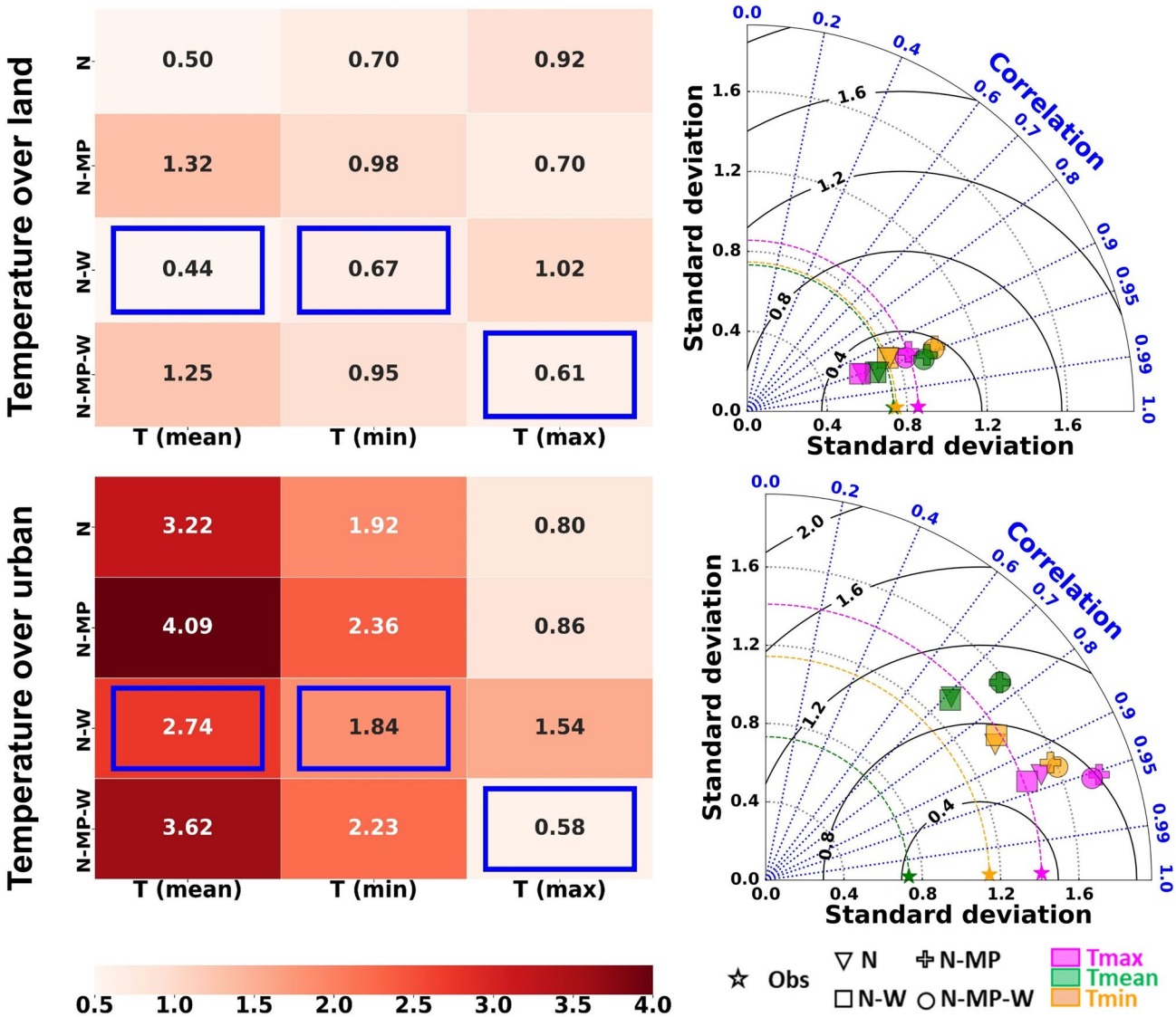

Figure 3. The statistical analysis averaged over the land (top row) and urban regions (bottom row) of the study area for the daily mean (T_{mean}), minimum (T_{min}), and maximum (T_{max}) temperature including, the unbiased root mean squared error (first column) and Taylor accuracy score (second column). The blue rectangles on the heatmaps denote the most accurate simulations. In the Taylor diagram, dotted gray lines connecting the *X*- and *Y*-axes denote the standard deviation; the dashed lines indicate the standard deviation of the observations (Obs), and the solid black radial lines represent the mean error, dotted blue radius connecting the center to arc axis show the Pearson correlation. N: Noah; N-MP: Noah MP; N-W: Noah + WUDAPT; and N-MP-W: Noah MP + WUDAPT simulations.

3. Results and Discussions

3.1. Model Evaluation

The model performance was evaluated over the entire land domain (i.e., by masking water bodies). The study region was divided into two: (a) land use categories except water (referred as land) and a subcategory of (b) urban areas (including all urban regions across Europe). The analysis (i.e., uRMSE and Taylor diagram) was carried out over these two categories by comparing the spatially averaged air temperature values from the WRF simulations against the E-OBS data set (Figures 3 and 4).

Figure 3 shows the uRMSE and Taylor diagrams of T_{mean}, T_{max}, and T_{min} for the WRF simulations. The Taylor diagrams show the relative performance and accuracy with respect to the observations (stars on the *x*-axis). The simulated values that lie nearest to their references (stars on the *x*-axis) signify the best agreement with the observations (higher correlation and lower error). The simulated values on the dashed arc (connecting *x*- and *y*-axis)

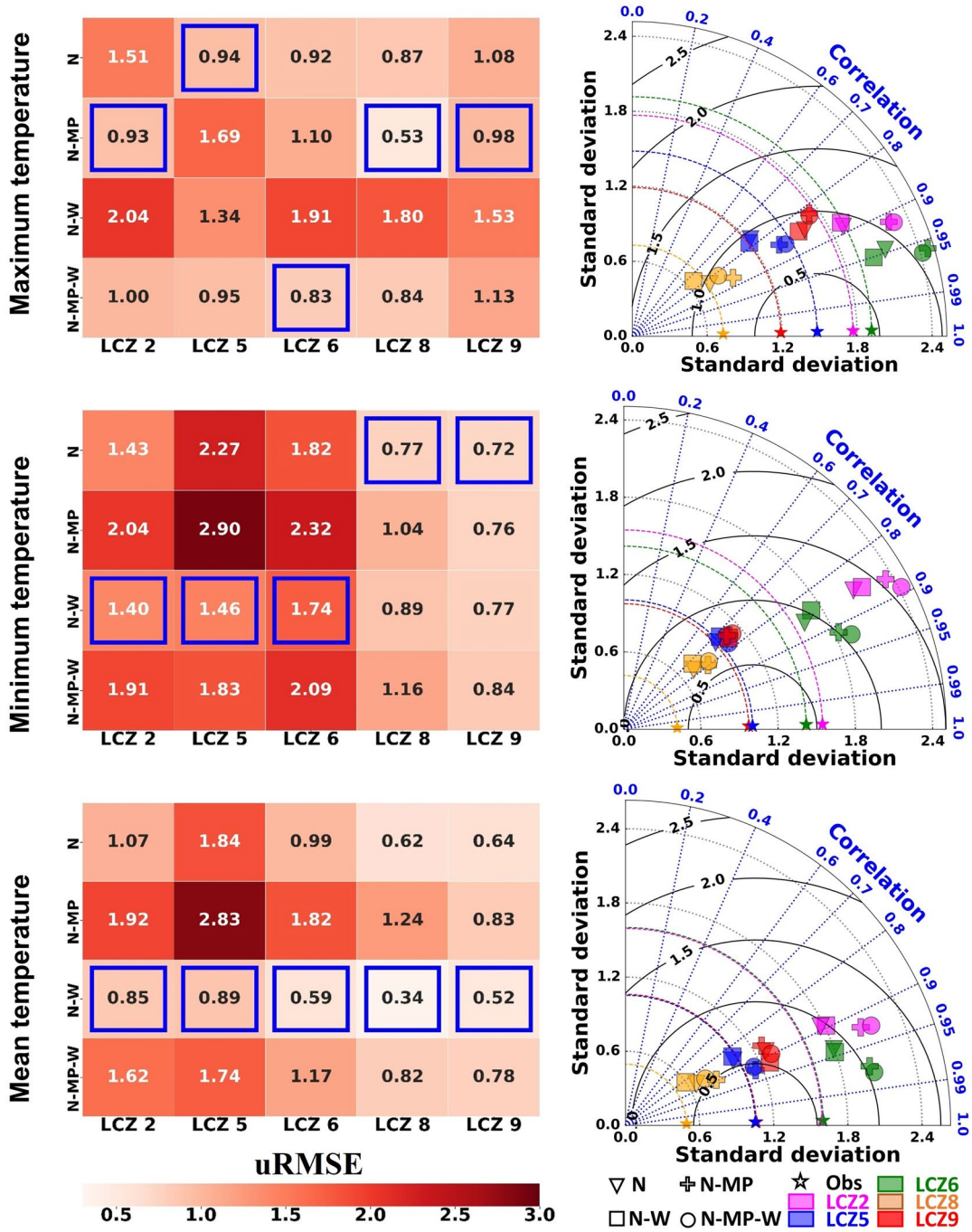

Figure 4. Same as Figure 3 but for different local climate zones. N: Noah, N-MP: Noah MP; N-W: Noah + WUDAPT; and N-MP-W: Noah MP + WUDAPT simulation.

represent closer variation amplitude with the observed values. The air temperature simulations over land (natural land also considering urban areas) showed a higher accuracy compared to the values simulated over urbanized areas. The heatmaps show that the N-W experiment simulated the T_{mean} and T_{min} with the lowest uRMSE, and T_{max} was simulated the best (lowest uRMSE) with the N-MP-W both for land and urban areas. When Noah was used (N and N-W simulations), the temperature variations were in closer agreement with the observations, while using Noah-MP (N-MP and N-MP-W simulations) yielded a better correlation with the observations (shown in Taylor Diagram). Incorporating LCZs produce more accurate simulations, particularly over the urban areas. The comparison of T_{mean}, T_{max}, and T_{min} over the LCZs are provided in Figure 4.

The LCZs comparison highlighted a more accurate simulation from the Noah compared to the Noah-MP for T_{mean} and T_{min}, while T_{max} was better simulated with Noah-MP. Incorporating LCZs in the simulations significantly reduced T_{mean} error in all LCZs (especially for LCZ 5). Nevertheless, the use of LCZs reduced the accuracy of T_{max} when paired with the land surface models (the N-W experiment). In the case of T_{min}, inconsistent results were observed when LCZs were incorporated in the simulations (as the error magnitude was reduced in the LCZ 2, LCZ 5, and LCZ 6 and increased in the LCZ 8 and LCZ 9). It is important to note that the urban stations are most likely to be located in pseudo-natural settings (such as parks) rather than over paved surfaces. This might explain the systematic bias in the urban simulations and the relative improvement over LCZ9, which is close to rural.

Overall, comparing the land surface parametrizations (N and N-MP), a higher positive bias was observed when the Noah-MP scheme was used. The Noah-MP simulated higher temperature due to the higher sensible heat (not shown here) than the Noah. When the LCZs were implemented into the LSMs (comparing N-W and N-MP-W), the simulation errors were reduced significantly. These improvements were more pronounced over the urban areas than in other regions. The performance (accuracy) of the experimented configurations to be coupled with the WRF could be ranked as Noah + WUDAPT > Noah > Noah-MP + WUDAPT > Noah-MP for the mean and minimum temperature and Noah-MP + WUDAPT > Noah-MP > Noah > Noah + WUDAPT for maximum temperature.

Consistent with our findings, Imran et al. (2018) have reported better average air temperature simulations from the Noah LSM compared to the Noah-MP model. The potential of WUDAPT in improving modeled temperatures with WRF has been highlighted in Leconte et al. (2015), Martilli et al. (2016), and Brousse et al. (2016), although these studies have considered only one city. It is important to note that the change in the representation of the urban areas (using LCZs) over the continent-scale reduces the simulation errors.

3.2. Time Series Analysis

3.2.1. Land and Urban

Figure 5 shows the time series of the mean, minimum, and maximum temperature averaged separately over land and urban regions of Europe for the entire simulation period. The simulations over land resulted in a closer agreement with the observations than the simulated values over the urban regions. Additionally, when Noah was selected as the LSM (N and N-W experiments), the mean and minimum daily temperatures were simulated more accurately. The maximum daily temperature was better simulated with Noah-MP (N-MP and N-MP-W simulations).

All the simulations showed a positive systematic bias (overestimation) compared to the observation except for the maximum temperature resulting from the N and N-W experiments. Coupling LCZs with the Noah and Noah-MP experiments reduced the magnitude of the simulated temperature. The reduction was more notable over the urban regions (particularly for the maximum daily temperature). Additional information for temperature values is provided in the form of the kernel density function shown in Figures S3–S5 in Supporting Information S1.

3.2.2. Local Climate Zones

The time series of the simulated mean air temperature over the urban region considering different LCZs is shown in Figure 6. The most accurate simulations were carried out for LCZs 8 and LCZ 9. Temperature simulations in LCZs 2 and LCZ 5 resulted in a higher bias compared to other LCZs. For LCZ 2 and LCZ 9, the N-W and N-MP-W simulations show nearly similar values to their paired experiments (N and N-MP, respectively). This similarity was attributed to the similar parameter values of LCZ 2 and LCZ 9 to the default (MODIS) values attributed to the urban and barren-sparsely vegetated class in N and N-MP simulations. A higher air temperature was found in LCZ 2 (reaching ≈300 K) due to the presence of a high urban roughness and more radiation absorption. On the contrary, LCZ 9 was the coolest regions for which during 19–22 of June 2017, the air temperature dropped below 283 K. The decreased temperature in the LCZ 9 was due to vegetation leading to more moisture availability (relative humidity) than the rest of the LCZs, which in turn could cause an increase in the latent heat flux and reduce the air temperature (more details are discussed in the following section).

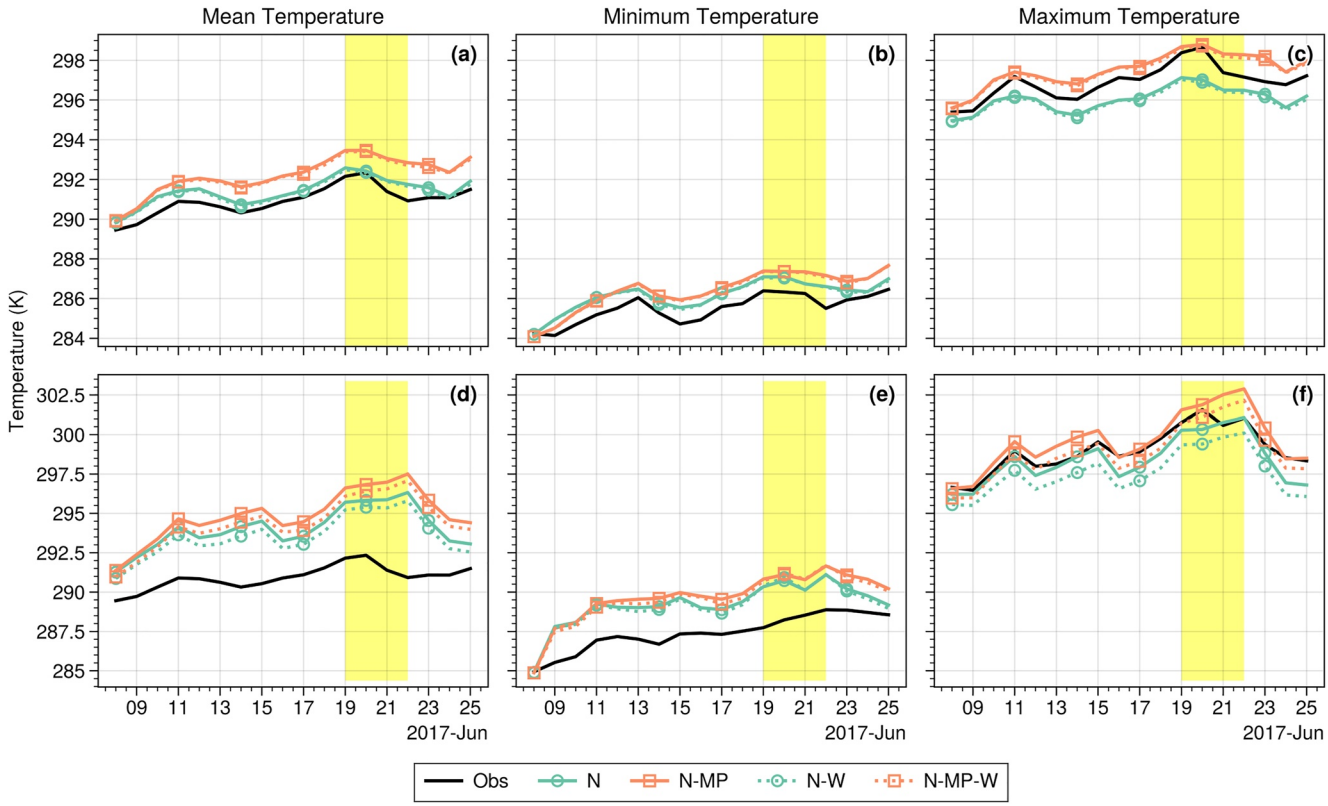

Figure 5. (a) Mean, (b) minimum, and (c) maximum temperature (K) over land and urban (d–f) from observations (Obs; solid black line), Noah (N; solid teal line with circle markers), Noah-MP (N-MP; solid orange line with square markers), Noah + WUDAPT (N-W; teal dashed line with circle markers), and Noah-MP + WUDAPT (N-MP-W; orange dashed line with square markers) simulations. The yellow shade shows the decaying phase of the heatwave period (19–22 June 2017).

3.3. Surface Energy Flux

The model estimates for the surface energy balance components were extracted, spatially averaged over the urban areas, and temporally averaged for the simulation period. The results are shown in Figure 7. Interestingly, net radiation is similar for all simulations except for an increase in N-W. By partitioning the net radiation into the sensible, latent, and ground heat flux (Figures 7a–7c), substantial differences among the simulated components were observed. The N and N-MP simulations followed a nearly similar pattern for surface energy balance components. The use of LCZs resulted in lower sensible heat flux and higher latent and ground heat flux simulations (more notably in the N-W experiments).

By implementing the urban LCZs, the sensible heat flux was reduced over 40% and 30% in the N-W, and N-MP-W simulations, respectively, and latent heat flux was increased 113% in N-W and 133% in N-MP-W, respectively. This significant change occurred because the urban region is a paved surface with low evapotranspiration (smaller latent heat flux) and allocate the available energy to heating the surface (increasing sensible and ground flux). The sensible heat flux simulated by the N-W and N-MP-W showed a maximum value of 281 and 334 W/m^2, respectively, while this value was 468 and 475 W/m^2 for N and N-MP simulations. Categorizing the urban areas into different LCZs (that includes more vegetation than MODIS) caused the simulations to have higher evapotranspiration, causing lower estimates for sensible and ground heat fluxes and affecting the simulated air temperature. The simulated latent heat flux showed a maximum value of 241 and 150 W/m^2 for the N-W and N-MP-W simulations, and 42 and 22 W/m^2 for the N, and N-MP simulations, respectively.

Additionally, altering the default LULC (in N and N-MP experiments) with LCZs (N-W and N-MP-W experiments) affected the overall 10-m wind speed within the urban regions. Figure 8a shows an increase in modeled wind speed using the WUDAPT parametrizations (N-W and N-MP-W). The changes in the wind speed and 2-m relative humidity using WUDAPT LULC only occurred on the magnitude, and the variability of them remained similar as simulated by the control experiments (N and N-MP). The wind speed showed 1.6 m/s, and relative

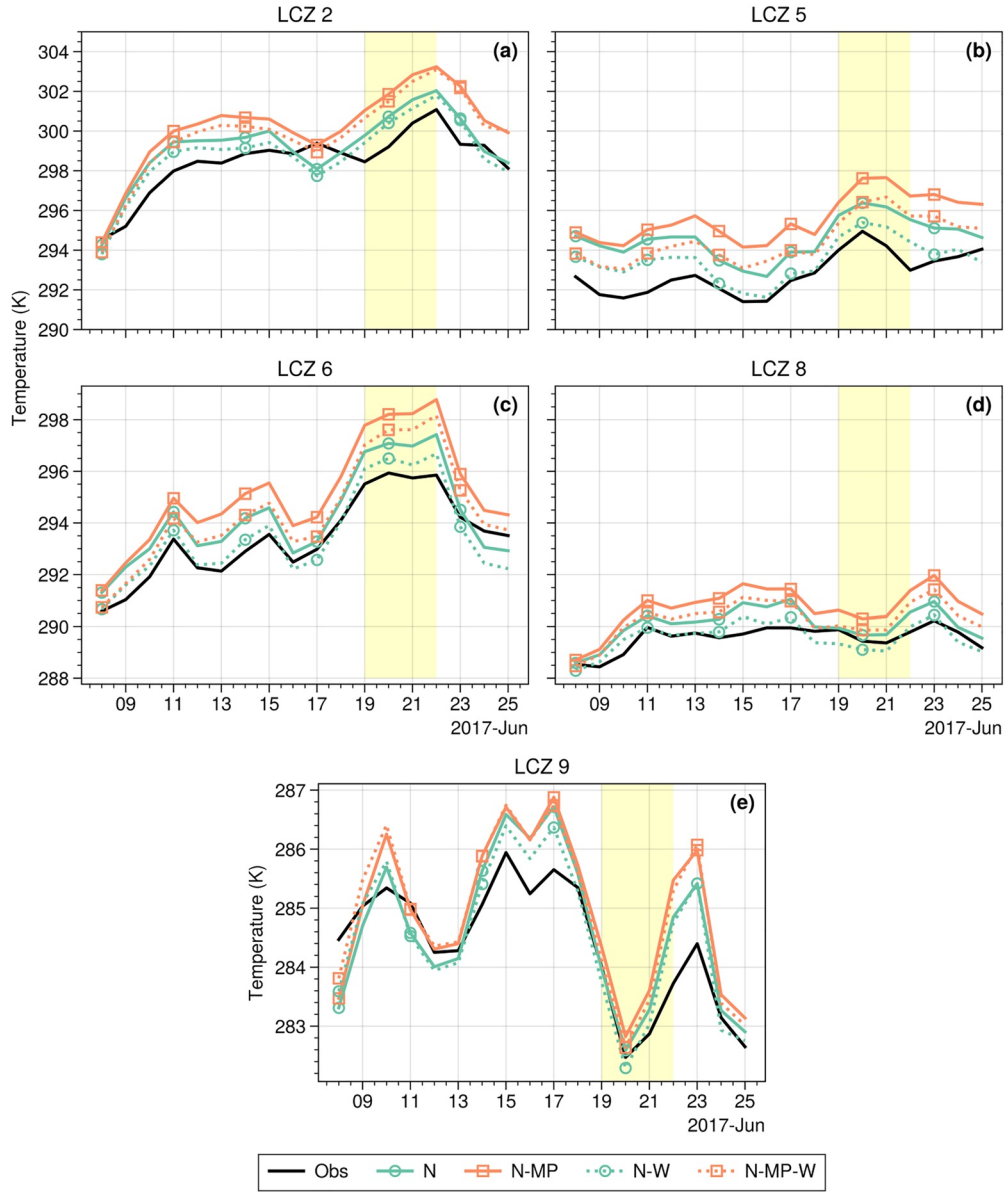

Figure 6. Mean temperature (K) over (a) compact mid-rise [local climate zones (LCZ 2)], (b) open mid-rise (LCZ 5), (c) open low-rise (LCZ 6), (d) sparsely built (LCZ 8), and (e) large low-rise (LCZ 9) from observations (Obs; solid black line), Noah (N; solid teal line with circle markers), Noah-MP (N-MP; solid orange line with square markers), Noah + WUDAPT (N-W; teal dashed line with circle markers), and Noah-MP + WUDAPT (N-MP-W; orange dashed line with square markers) simulations. The yellow shade indicates the decaying phase of the heatwave period (19–22 June 2017).

humidity showed 5%–8% of systematic difference between the paired experiments (N and N-MP experiments vs. N-W and N-MP-W experiments).

During the heatwave event, all four experiments depicted a reduction in the relative humidity and wind speed (not consistent for all LCZs). During the decay period (19–22 June 2017), the average wind speed for the WUDAPT simulations was approximately 60% higher than the N and N-MP simulations. Higher wind speed with the incorporation of the WUDAPT caused more energy exchange and led to lower (and more accurate) air temperature in the N-W and N-MP-W simulations (discussed above in Figures 6 and 7).

Overall, the similar wind speed using the different LSMs suggested that the choice of LSMs did not significantly affect the wind speed simulations. However, the choice of LULC showed a more highlighted role given the

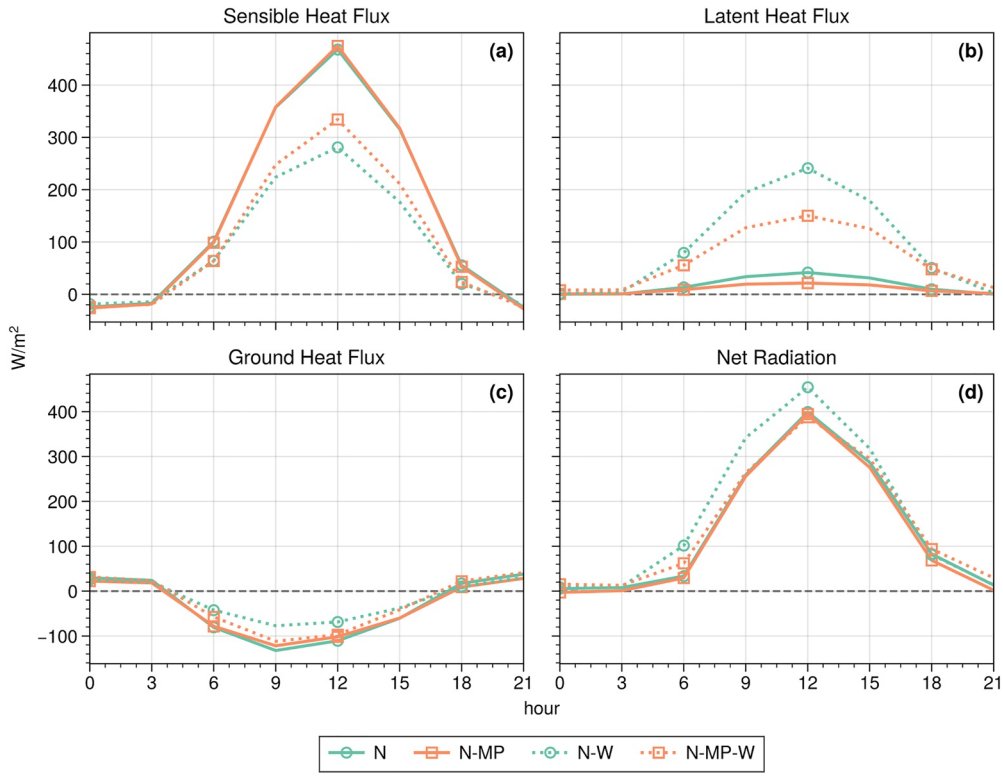

Figure 7. Diurnal (a) sensible heat flux, (b) latent heat flux, (c) ground heat flux, and (d) net radiation during the simulation period over the urban regions for Noah (N; solid teal line with circle markers), Noah-MP (N-MP; solid orange line with square markers), Noah + WUDAPT (N-W; teal dashed line with circle markers), and Noah-MP + WUDAPT (N-MP-W) simulations.

significant difference in the wind speed values in the N-W and N-MP-W experiments compared to the N and N-MP experiments. It should be noted that these changes were not consistent among the different LCZs. Higher wind speeds were observed over the LCZs 5, LCZ 6, and LCZ 8 (Figure 9). For very compact and very sparse

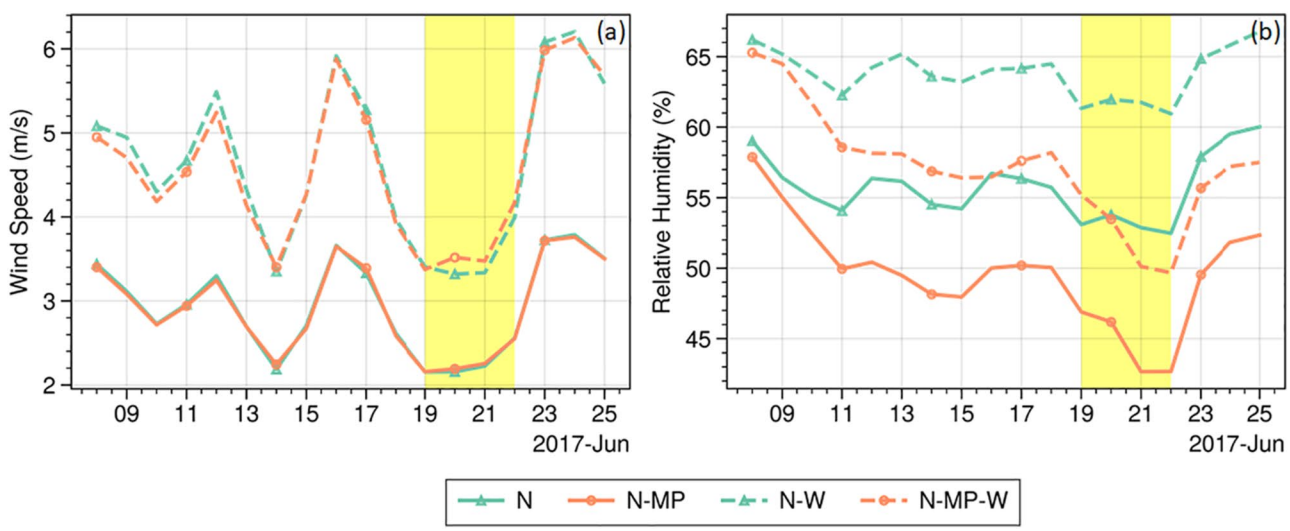

Figure 8. Time series of (a) average 10-m wind speed and (b) 2-m relative humidity over the urban regions of the study area (Europe) during the 2017 heatwave. Noah (N; solid teal line with circle markers), Noah-MP (N-MP; solid orange line with square markers), Noah + WUDAPT (N-W; teal dashed line with circle markers), and Noah-MP + WUDAPT (N-MP-W; orange dashed line with square markers) simulations. The yellow shade indicates the decaying phase of the heatwave period (19–22 June 2017).

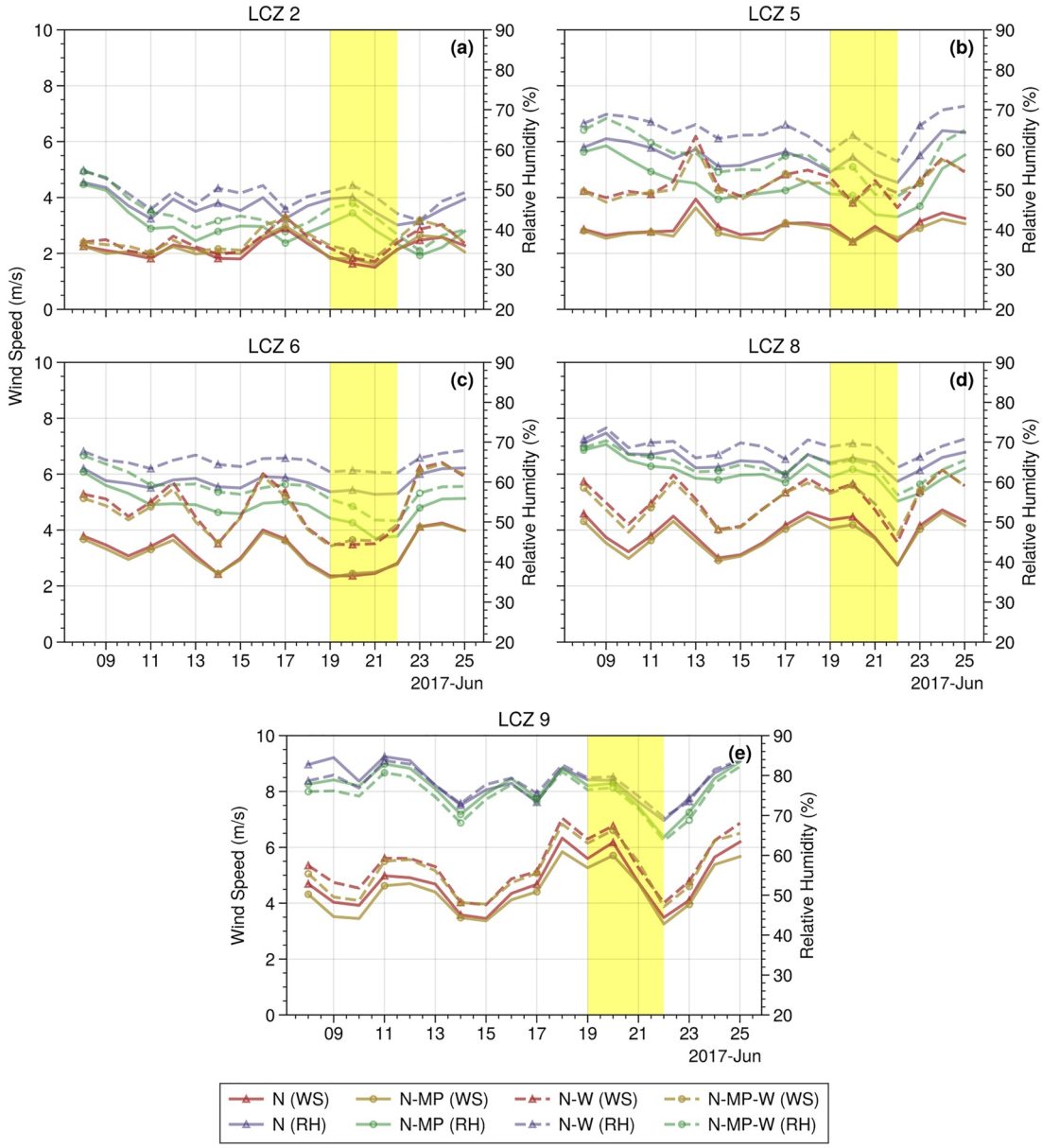

Figure 9. Time series of average wind speed (WS) and relative humidity (RH) over the (a) compact mid-rise [local climate zones (LCZ 2)], (b) open mid-rise (LCZ 5), (c) open low-rise (LCZ 6), (d) sparsely built (LCZ 8), and (e) large low-rise (LCZ 9) of the study area (Europe) during the 2017 heatwave. For Noah (N), Noah-MP (N-MP), Noah + WUDAPT (N-W), and Noah-MP + WUDAPT (N-MP-W) simulations.

built-up areas (LCZs 2 and LCZ 9), the wind speed simulations did not significantly differ among the experiments. Since, majority of the urban regions of the study area is covered by LCZ 6 (77%; lower roughness length compared to MODIS), wind speed values were higher. The increased wind speed and moisture content over the urban regions simulated by the N-W and N-MP-W experiments affected the amount of advection and changed the temperatures outside the urban regions.

In the case of relative humidity, both LSM and LULC choices have affected the simulated values (given the difference between the simulated trends from the experiments), although this contribution was not similar among different LCZs (Figure 9). For example, in LCZ 9, the simulated relative humidity remained similar among the experiments, while in LCZ 5 and LCZ 6, more notable differences were observed (Figure 9). Contrary, the wind speed, and relative humidity during the decay period were increased in LCZs 8 and LCZ 9. Higher wind speed

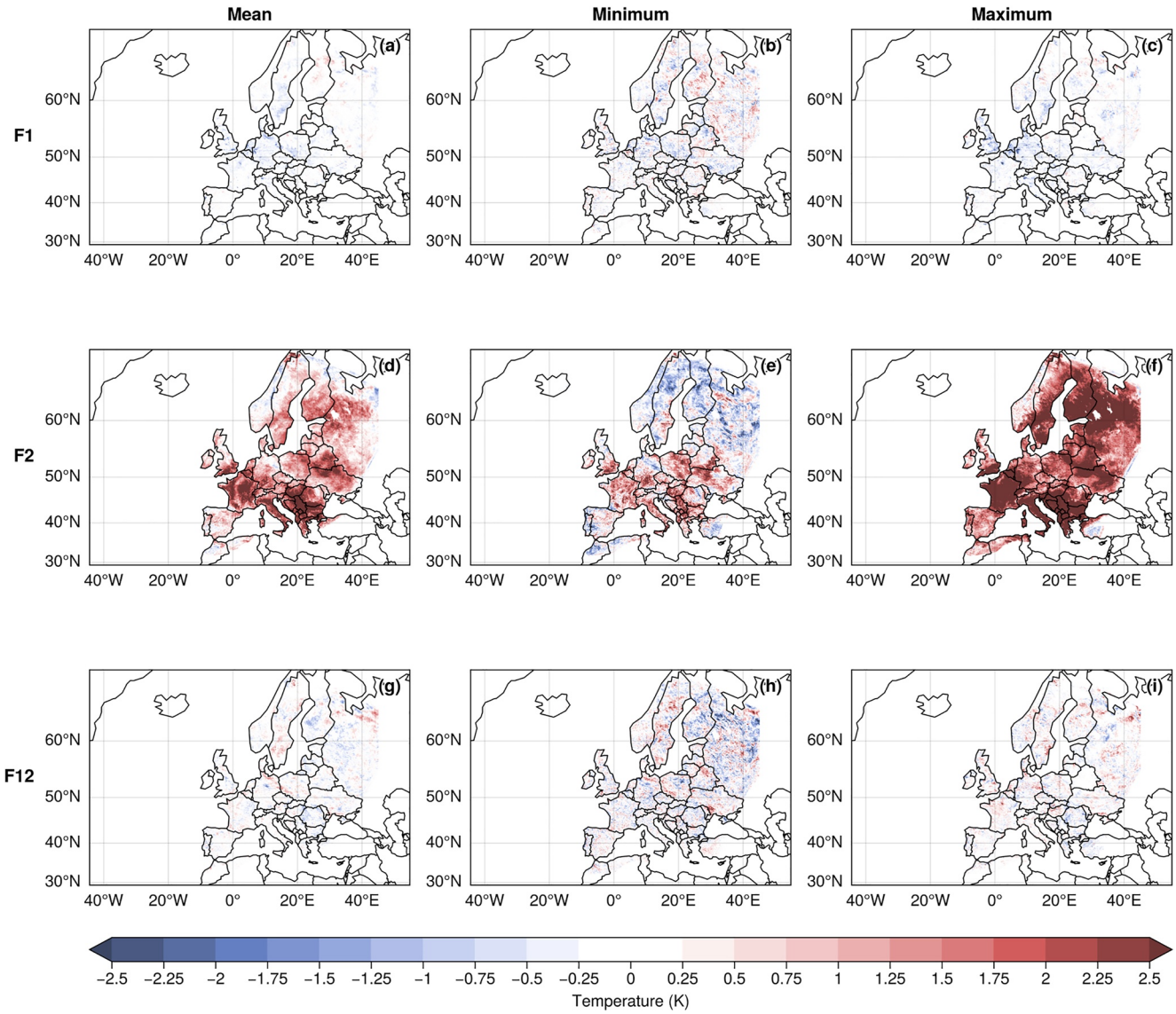

Figure 10. Factor separation based on the 0.95 quantile for the mean (a, d, g), minimum (b, e, h), and maximum (c, f, i) temperature over Europe during 08–25 June 2017. (a–c) F1 is the effect of land use/land cover (LULC), (d–f) F2 is the effect of land surface parameterization, and (g–i) F12 is the combined effect of LULC and land surface parameterization.

simulated in these two LCZs likely caused more energy exchange, and thus, the simulated air temperature showed increased during the heatwave period in these LCZs (Figure 6).

3.4. Factor Separation and Spatial Analysis

3.4.1. Air Temperature

Figure 10 shows the factor separation of the 0.95 quantile of mean, minimum, and maximum daily temperature from the entire simulation period. The 0.05 quantile and mean of minimum, maximum, and mean daily temperature are shown in Figures S13 and S14 in Supporting Information S1, respectively. Figures 10a–10f (also Figures S13 and S14 in Supporting Information S1) suggests that the impact of parametrization (F2) is more significant than that of urban land use (F1). Shifting from the default LULC to WUDAPT (F1) had a marginal cooling impact over most of Europe and more notably impacted the maximum and minimum temperature simulations than the mean temperature. Changing the LSM from Noah to Noah-MP translated to strong warming over most of

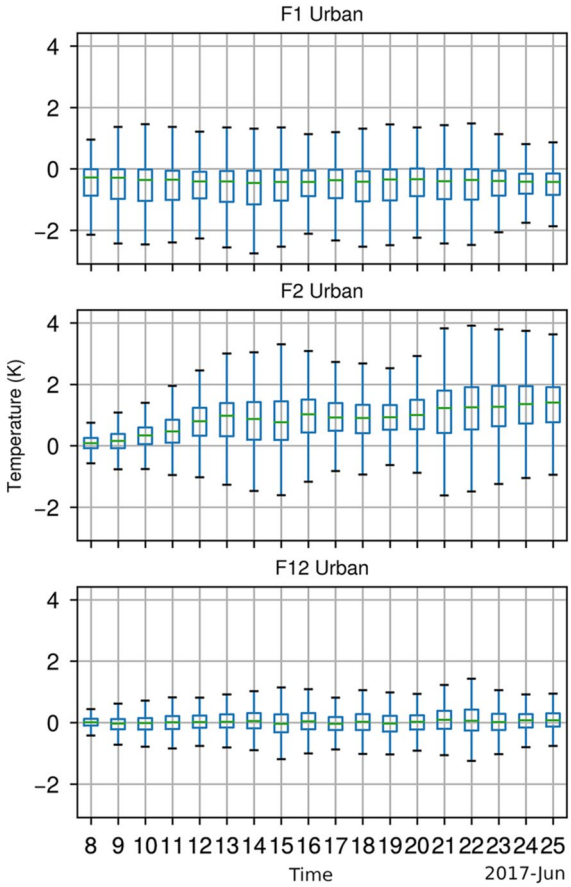

Figure 11. Box plots of daily mean air temperature changes over urban regions illustrated by box-plots for the F1, F2, and F12 factors during the 2017 heatwave. F1 is the effect of land use/land cover (LULC), F2 is the effect of land surface parameterization, and F12 is the combined effect of LULC and land surface parameterization.

Europe while there were instances of decreasing temperature (particularly in minimum temperature simulations over Northern Europe). The temperature variations resulting from the LSMs (Noah and Noah-MP) were due to the semi-tile approach implemented in Noah-MP. The Noah LSM considers a single linearized energy balance equation representing combined ground—vegetation surface, while the Noah-MP considers a three-layer energy—mass balance model. LSM and LULC (F12) combined effect showed warming, more notably on the minimum and maximum temperature simulations and in Western Europe.

The air temperature changes across the continent when incorporating LCZs indicates that urban areas affect the simulations outside the urban grid cells. Notably more than 1.9%, 4.2%, and 5.5% of the total land area witnessed a change of more than 1 K of mean, minimum, and maximum air temperature change due to the urban LCZs. With the inclusion of LCZs there is increased urban heterogeneity and more vegetative area (variable urban fraction 0.3–1.0) than the default LULC (constant urban fraction of 0.9). The resulting impact on surface meteorology is noted through a 7% net mean increase in relative humidity combined with an increase in the surface winds, which is expected due to the relative decrease in urban roughness (LCZs compared to default). An interesting impact is the change in the temperatures beyond the urban grids likely due to advection. Note that, in the N and N-MP (as well as in N-W and N-MP-W) the urban grids (urban or LCZs grids) and urban parameterization remain the same, further highlighting that the urban grids affecting neighboring grids and vice-versa (as a two-way feedback).

As depicted in Figure 10, the impact of LSMs and urban land use were spatially different. The variability over urban regions is illustrated as time series box plots shown in Figure 11. The impact of LCZ (F1) showed an overall decrease in temperature in most regions. On comparing with the urban areas, a decrease in ≈0.5 K is observed. It can also be noted that the change in temperature from F1 extends outside the boundaries of the urban regions. The impact of parameterization (F2) increases the temperature in most of the regions. Interestingly, for the urban regions, the changes in the temperature due to F2 are more than the F1, while using the same urban canopy model. The combined effect of LCZs and LSMs shows mixed changes in the temperature. The temperature variation is limited between −1.2 and 1.4 K from the Noah simulation for the urban areas.

3.4.2. Heat Index

Figures 12a–12d shows maximum HI simulated from the four different configurations during the heatwave event. The differences between these simulations were shown by the factor separation analysis (Figures 12e and 12g). The factor separation results were aligned with the findings described on the temperature variations (previous section). Using LCZs caused a lower HI over most of Europe except in some regions. The F2 factor (the impact of land models, Noah vs. Noah-MP) showed a strong warming impact over the entire region. The changes in the HI represent the changes that occurred from the combined effect of the temperature and relative humidity. The mean (maximum) of maximum HI from N is 21.6°C (43.0°C), N-MP is 22.3°C (46 .3°C), N-W is 21.5°C (44.3°C), and N-W-MP is 22.2°C (51.1°C). The maximum (minimum) values of the HI for F1, F2, and F12 are 9.4°C (−5.6°C), 8.6°C (−6.4°C), and 11.5°C (−9.2°C), respectively.

Over the urban regions, in F1, there are several occurrences of maximum HI change of more than 2°C (see Figure S15 in Supporting Information S1). On the other hand, F2 increases mean and maximum HI values up to 4.5°C, while more than 50% of grids show almost no change in minimum HI values. F12 shows a mixed pattern from F1 and F2. The maximum and HI values range from −3.5°C to 4°C, mean values are concentrated between −0.5°C and 0.5°C, and more than 50% of grids show no change in minimum values. Overall, maximum HI values are

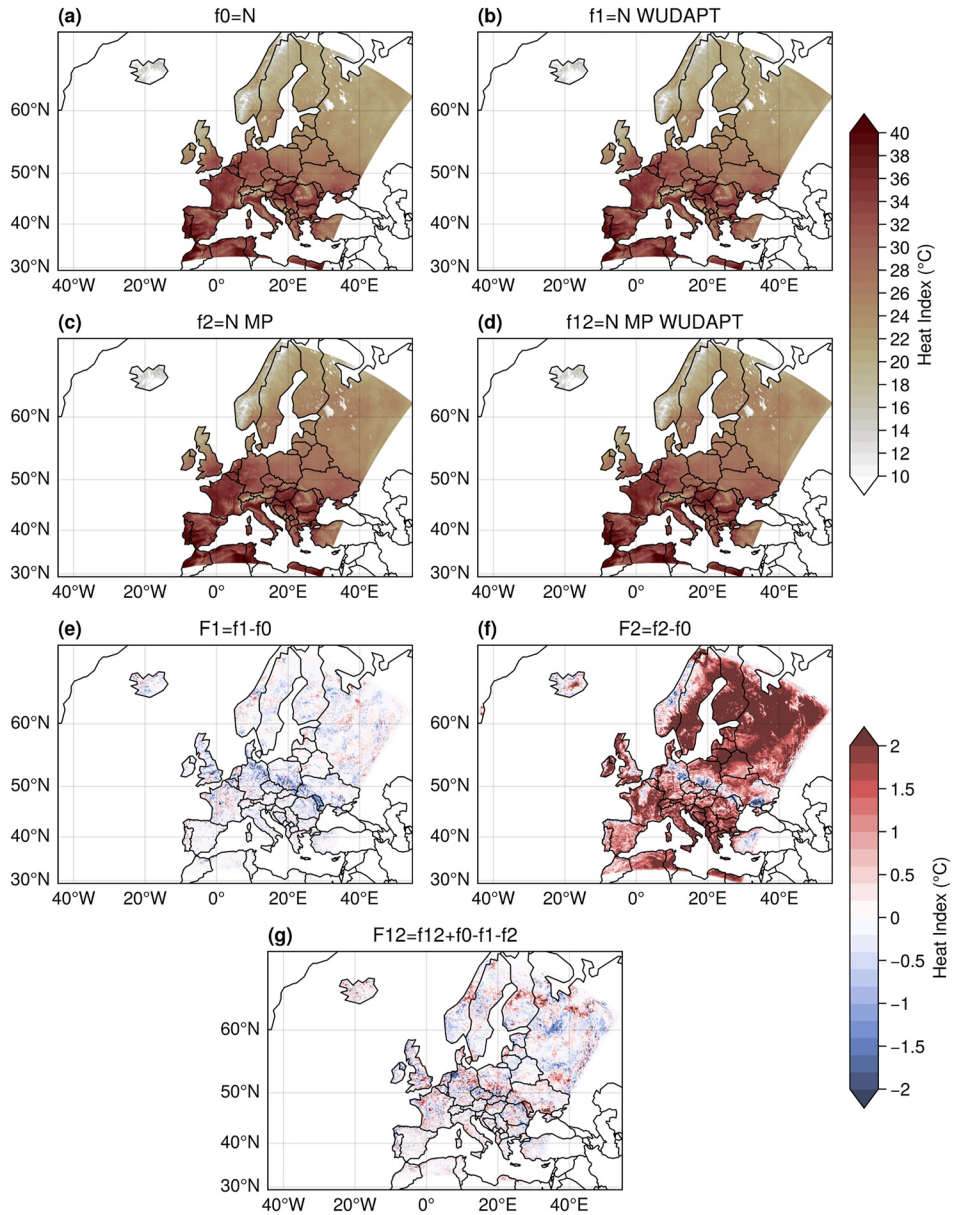

Figure 12. Maximum heat index over the study area (Europe) during the 2017 heatwave and its factor separation (F1, F2, and F12). (N: Noah, N-MP: Noah MP; N-W: Noah + WUDAPT; and N-MP-W: Noah MP + WUDAPT; F1 is the effect of land use/land cover (LULC), F2 is the effect of land surface parameterization, and F12 is the combined effect of LULC and land surface parameterization.

most affected by the changes in the urban surface properties and land surface parameterization, thus affecting mean, while the minimum HI values are least affected.

4. Conclusions

In this study, we assessed the impact of LCZs and LSM parameterizations on simulating an extreme heatwave event over Europe. Accordingly, we simulated the 2017 heatwave event using WRF and considering four configurations. We first simulated the heatwave using the WRF model coupled to the Noah and Noah-MP LSMs supported with the default LULC to evaluate the effect of LSMs and then successfully replaced the default LULC in the Noah and Noah-MP with the WUDAPT LULC to evaluate the impact of detailed urban LCZs on the simulations. The key findings of this work are summarized as follows:

1. The combination of Noah with WUDAPT (the N-W experiment) simulated the air temperature more accurately than other experiments. The representation of urban heterogeneity through the LCZs represented the local temperature variation within the urban areas and improved the overall temperature simulation for such a large-scale event. Also, the performance is improved by using WUDAPT for both Noah and Noah MP.
2. The resulting accuracy from the N-W simulations was attributed to two major factors. The first factor was the parameterizations used in the Noah model as the temperature simulated by Noah was closer to the observations compared to the warmer temperature simulated by the Noah-MP scheme. Second, the incorporation of LCZs into the simulations altered the surface energy partitioning (caused more energy allocation to latent heat flux due to larger vegetated fractions in the urban areas) and reduced (improved) the simulated air temperature.
3. A more detailed representation of urban areas by incorporating LCZs revealed an important finding that the urban areas could affect the air temperature outside their regions. More specifically, incorporating LCZs reduced surface roughness, increased moisture (due to vegetation), and wind speed; thus altering the air temperature outside of the urban periphery. The N and N-MP (also N-W and N-MP-W) simulations show the impact of surrounding areas on the urban grids; thus, a two-way feedback to and from the urban environments.

Our findings show the potential of using LCZs in the current atmospheric models to enhance the urban areas' representation and more accurate simulations. This improvement is significant, considering the intensification of the heatwaves in the mid-latitudes and the increasing fatality risk per each degree temperature increase. The study provides the first results to show the use of LCZ improves large-scale WRF simulation. Urban planners and policymakers can employ our findings in more generic frameworks to evaluate the impact of such events on the ecosystem, human health and plan accordingly for a particular LCZ (instead of treating an urban area as a whole).

Data Availability Statement

The WRF model outputs used for analysis in the study will be available at Zenodo via https://doi.org/10.5281/zenodo.5511612 with Creative Commons Attribution 4.0 International license.

Acknowledgments
This work benefited in part through, Project MoES/PAMC/H&C/36/2013-PC-II from the Ministry of Earth Sciences, India; Department of Science & Technology (SPLICE - Climate Change Programme), India, Project DST/CCP/CoE/140/2018, Grant: 10013072 (UC ID: 18192442); US National Science Foundation OAC-1835739, AGS-1522492, USDA Hatch Project 1007699; NASA IDS Grant Number: 80NSSC20K1262 and 80NSSC20K1268; USDA NIFA Grant 2015-67003-23460. Matthias Demuzere was supported by the ENLIGHT project, funded by the German Research Foundation (DFG) under grant No. 437467569. The lead author acknowledges the SERB Overseas Visiting Doctoral Fellowship [SB/59/Z-03/2017-XI(2018-19)] for a 1-year research visit to Purdue University.

References

An der Heiden, M., Muthers, S., Niemann, H., Buchholz, U., Grabenhenrich, L., & Matzarakis, A. (2020). Heat-related mortality: An analysis of the impact of heatwaves in Germany between 1992 and 2017. *Deutsches Ärzteblatt International*, *117*(37), 603–609. https://doi.org/10.3238/arztebl.2020.0603

Anderson, G. B., & Bell, M. L. (2010). Heat waves in the United States: Mortality risk during heat waves and effect modification by heat wave characteristics in 43 U.S. communities. *Environmental Health Perspectives*, *119*(2), 210–218. https://doi.org/10.1289/ehp.1002313

Bougeault, P., & Lacarrere, P. (1989). Parameterization of orography-induced turbulence in a mesobeta – scale model. *Monthly Weather Review*, *117*(8), 1872–1890. https://doi.org/10.1175/1520-0493(1989)117<1872:pooiti>2.0.co;2

Brousse, O., Martilli, A., Foley, M., Mills, G., & Bechtel, B. (2016). WUDAPT, an efficient land use producing data tool for mesoscale models? Integration of urban LCZ in WRF over Madrid. *Urban Climate*, *17*, 116–134. https://doi.org/10.1016/j.uclim.2016.04.001

Chen, F., & Dudhia, J. (2001). Coupling an advanced land surface–hydrology model with the Penn state–NCAR MM5 modeling system. Part I: Model implementation and sensitivity. *Monthly Weather Review*, *129*(4), 569–585. https://doi.org/10.1175/1520-0493(2001)129<0569:caalsh>2.0.co;2

Chen, F., Kusaka, H., Bornstein, R., Ching, J., Grimmond, C., Grossman-Clarke, S., et al. (2011). The integrated WRF/urban modelling system: Development, evaluation, and applications to urban environmental problems. *International Journal of Climatology*, *31*(2), 273–288. https://doi.org/10.1002/joc.2158

Chen, F., Mitchell, K., Schaake, J., Xue, Y., Pan, H. L., Koren, V., et al. (1996). Modeling of land surface evaporation by four schemes and comparison with FIFE observations. *Journal of Geophysical Research*, *101*(D3), 7251–7268. https://doi.org/10.1029/95jd02165

Ching, J., Aliaga, D., Mills, G., Masson, V., See, L., Neophytou, M., et al. (2019). Pathway using WUDAPT's digital synthetic city tool towards generating urban canopy parameters for multi-scale urban atmospheric modeling. *Urban Climate*, *28*, 100459. https://doi.org/10.1016/j.uclim.2019.100459

Ching, J., Mills, G., Bechtel, B., See, L., Feddema, J., Wang, X., et al. (2018). WUDAPT: An urban weather, climate, and environmental modeling infrastructure for the Anthropocene. *Bulletin of the American Meteorological Society*, *99*(9), 1907–1924. https://doi.org/10.1175/bams-d-16-0236.1

Chou, M.-D., & Suarez, M. J. (1994). An efficient thermal infrared radiation parameterization for use in general circulation models. *NASA Technical Memorandum 104606*, *3*, 85.

Cornes, R. C., vander Schrier, G., vander Besselaar, E. J., & Jones, P. D. (2018). An ensemble version of the E-OBS temperature and precipitation data sets. *Journal of Geophysical Research: Atmospheres*, *123*(17), 9391–9409. https://doi.org/10.1029/2017jd028200

Croce, P., Formichi, P., Landi, F., Mercogliano, P., Bucchignani, E., Dosio, A., & Dimova, S. (2018). The snow load in Europe and the climate change. *Climate Risk Management*, *20*, 138–154. https://doi.org/10.1016/j.crm.2018.03.001

Demuzere, M., Bechtel, B., Middel, A., & Mills, G. (2019a). *European LCZ map*. Figshare. https://doi.org/10.6084/m9.figshare.13322450.v1

Demuzere, M., Bechtel, B., Middel, A., & Mills, G. (2019b). Mapping Europe into local climate zones. *PLoS ONEne*, *14*(4), e0214474. https://doi.org/10.1371/journal.pone.0214474

Demuzere, M., Harshan, S., Järvi, L., Roth, M., Grimmond, C., Masson, V., et al. (2017). Impact of urban canopy models and external parameters on the modelled urban energy balance in a tropical city. *Quarterly Journal of the Royal Meteorological Society*, *143*(704), 1581–1596. https://doi.org/10.1002/qj.3028

Ek, M., Mitchell, K., Lin, Y., Rogers, E., Grunmann, P., Koren, V., et al. (2003). Implementation of Noah land surface model advances in the National Centers for Environmental Prediction operational mesoscale Eta model. *Journal of Geophysical Research*, *108*(D22), 8851. https://doi.org/10.1029/2002jd003296

Hammerberg, K., Brousse, O., Martilli, A., & Mahdavi, A. (2018). Implications of employing detailed urban canopy parameters for mesoscale climate modelling: A comparison between WUDAPT and GIS databases over Vienna, Austria. *International Journal of Climatology*, *38*(51), e1241–e1257. https://doi.org/10.1002/joc.5447

Hartfield, G., Blunden, J., & Arndt, D. S. (2018). State of the climate in 2017. *Bulletin of the American Meteorological Society*, *99*(8), Si–S310. https://doi.org/10.1175/2018bamsstateoftheclimate.1

Hertwig, D., Grimmond, S., Hendry, M. A., Saunders, B., Wang, Z., Jeoffrion, M., et al. (2020). Urban signals in high-resolution weather and climate simulations: Role of urban land-surface characterisation. *Theoretical and Applied Climatology*, *142*(1–2), 701–728. https://doi.org/10.1007/s00704-020-03294-1

Hong, S. Y., & Lim, J. O. J. (2006). The WRF single-moment 6-class microphysics scheme (WSM6). *Asia-Pacific Journal of Atmospheric Sciences*, *42*(2), 129–151.

Imran, H. M., Kala, J., Ng, A. W. M., & Muthukumaran, S. (2018). An evaluation of the performance of a WRF multi-physics ensemble for heatwave events over the city of Melbourne in southeast Australia. *Climate Dynamics*, *50*(7–8), 2553–2586. https://doi.org/10.1007/s00382-017-3758-y

IPCC. (2013). *Climate change 2013: The physical science basis: Working group I contribution to the fifth assessment report of the Intergovernmental Panel on Climate Change*. Cambridge University Press.

IPCC. (2014). *Climate Change 2014–Impacts, adaptation and vulnerability: Part B: Regional aspects: Working group II contribution to the IPCC fifth assessment report* (Vol. 2, pp. 1267–1326). Cambridge University Press. https://doi.org/10.1017/CBO9781107415386.003

Kain, J. S. (2004). The Kain–Fritsch convective parameterization: An update. *Journal of Applied Meteorology*, *43*(1), 170–181. https://doi.org/10.1175/1520-0450(2004)043<0170:tkcpau>2.0.co;2

Krauskopf, T., & Huth, R. (2020). Temperature trends in Europe: Comparison of different data sources. *Theoretical and Applied Climatology*, *139*(3), 1305–1316. https://doi.org/10.1007/s00704-019-03038-w

Kyselỳ, J., & Plavcová, E. (2010). A critical remark on the applicability of E-OBS European gridded temperature data set for validating control climate simulations. *Journal of Geophysical Research*, *115*(D23), D23118. https://doi.org/10.1029/2010JD014123

Leconte, F., Bouyer, J., Claverie, R., & Pétrissans, M. (2015). Estimation of spatial air temperature distribution at sub-mesoclimatic scale using the LCZ scheme and mobile measurements. In *Proceedings of the 9th International Conference on Urban Climate (ICUC9) jointly with 12th symposium on the urban environment*.

Li, D., & Bou-Zeid, E. (2013). Synergistic interactions between urban heat islands and heat waves: The impact in cities is larger than the sum of its parts. *Journal of Applied Meteorology and Climatology*, *52*(9), 2051–2064. https://doi.org/10.1175/jamc-d-13-02.1

Lorenz, R., Stalhandske, Z., & Fischer, E. M. (2019). Detection of a climate change signal in extreme heat, heat stress, and cold in Europe from observations. *Geophysical Research Letters*, *46*(14), 8363–8374. https://doi.org/10.1029/2019gl082062

Mahmood, R., Pielke, R. A., Hubbard, K. G., Niyogi, D., Dirmeyer, P. A., Mcalpine, C., et al. (2014). Land cover changes and their biogeophysical effects on climate. *International Journal of Climatology*, *34*(4), 929–953. https://doi.org/10.1002/joc.3736

Martilli, A., Brousse, O., & Ching, J. (2016). Urbanized WRF modeling using WUDAPT. In *Technical report March, Cientro de Investigaciones Energeticas Medioambientales y Tecnologicas*. (CIEMAT).

Martilli, A., Clappier, A., & Rotach, M. W. (2002). An urban surface exchange parameterisation for mesoscale models. *Boundary-Layer Meteorology*, *104*(2), 261–304. https://doi.org/10.1023/a:1016099921195

Miralles, D. G., Teuling, A. J., Van Heerwaarden, C. C., & De Arellano, J. V.-G. (2014). Mega-heatwave temperatures due to combined soil desiccation and atmospheric heat accumulation. *Nature Geoscience*, *7*(5), 345–349. https://doi.org/10.1038/ngeo2141

Mlawer, E. J., Taubman, S. J., Brown, P. D., Iacono, M. J., & Clough, S. A. (1997). Radiative transfer for inhomogeneous atmospheres: RRTM, a validated correlated-k model for the longwave. *Journal of Geophysical Research*, *102*(D14), 16663–16682. https://doi.org/10.1029/97jd00237

Molnár, G., Gyöngyösi, A. Z., & Gál, T. (2019). Integration of an LCZ-based classification into WRF to assess the intra-urban temperature pattern under a heatwave period in Szeged, Hungary. *Theoretical and Applied Climatology*, *138*(1), 1139–1158. https://doi.org/10.1007/s00704-019-02881-1

Montandon, L. M., Fall, S., Pielke Sr, R. A., & Niyogi, D. (2011). Distribution of landscape types in the global historical climatology network. *Earth Interactions*, *15*(6), 1–24. https://doi.org/10.1175/2010ei371.1

Nissen, K. M., & Ulbrich, U. (2017). Increasing frequencies and changing characteristics of heavy precipitation events threatening infrastructure in europe under climate change. *Natural Hazards and Earth System Sciences*, *17*(7), 1177–1190. https://doi.org/10.5194/nhess-17-1177-2017

Niu, G. Y., Yang, Z. L., Mitchell, K. E., Chen, F., Ek, M. B., Barlage, M., et al. (2011). The community Noah land surface model with multiparameterization options (Noah-MP): 1. Model description and evaluation with local-scale measurements. *Journal of Geophysical Research*, *116*(12), D12109. https://doi.org/10.1029/2010jd015139

Niyogi, D., Holt, T., Zhong, S., Pyle, P. C., & Basara, J. (2006). Urban and land surface effects on the 30 July 2003 mesoscale convective system event observed in the southern Great Plains. *Journal of Geophysical Research*, *111*(D19), D19107. https://doi.org/10.1029/2005jd006746

Oke, T. R. (1982). The energetic basis of the urban heat island. *Quarterly Journal of the Royal Meteorological Society*, *108*(455), 1–24. https://doi.org/10.1002/qj.49710845502

Patel, P., Karmakar, S., Ghosh, S., & Niyogi, D. (2020). Improved simulation of very heavy rainfall events by incorporating WUDAPT urban land use/land cover in WRF. *Urban Climate*, *32*, 100616. https://doi.org/10.1016/j.uclim.2020.100616

Politi, N., Nastos, P., Sfetsos, A., Vlachogiannis, D., & Dalezios, N. (2018). Evaluation of the AWR-WRF model configuration at high resolution over the domain of Greece. *Atmospheric Research*, *208*, 229–245. https://doi.org/10.1016/j.atmosres.2017.10.019

Powers, J. G., Klemp, J. B., Skamarock, W. C., Davis, C. A., Dudhia, J., Gill, D. O., et al. (2017). The weather research and forecasting model: Overview, system efforts, and future directions. *Bulletin of the American Meteorological Society*, *98*(8), 1717–1737. https://doi.org/10.1175/bams-d-15-00308.1

Robine, J.-M., Cheung, S. L. K., Le Roy, S., Van Oyen, H., Griffiths, C., Michel, J.-P., & Herrmann, F. R. (2008). Death toll exceeded 70,000 in Europe during the summer of 2003. *Comptes Rendus Biologies*, *331*(2), 171–178. https://doi.org/10.1016/j.crvi.2007.12.001

Rothfusz, L. P., & Headquarters, N. S. R. (1990). *The heat index equation (or, more than you ever wanted to know about heat index)*. National Oceanic and Atmospheric Administration, National Weather Service, Office of Meteorology.

Salamanca, F., & Martilli, A. (2010). A new building energy model coupled with an urban canopy parameterization for urban climate simulations—Part II. Validation with one dimension off-line simulations. *Theoretical and Applied Climatology*, *99*(3), 345–356. https://doi.org/10.1007/s00704-009-0143-8

Salamanca, F., Martilli, A., Tewari, M., & Chen, F. (2011). A study of the urban boundary layer using different urban parameterizations and high-resolution urban canopy parameters with WRF. *Journal of Applied Meteorology and Climatology*, *50*(5), 1107–1128. https://doi.org/10.1175/2010jamc2538.1

Sánchez-Benítez, A., García-Herrera, R., Barriopedro, D., Sousa, P. M., & Trigo, R. M. (2018). June 2017: The earliest European summer mega-heatwave of reanalysis period. *Geophysical Research Letters*, *45*(4), 1955–1962. https://doi.org/10.1002/2018gl077253

Schwarz, N., & Manceur, A. M. (2015). Analyzing the influence of urban forms on surface urban heat islands in Europe. *Journal of the Urban Planning and Development Division*, *141*(3), A4014003. https://doi.org/10.1061/(asce)up.1943-5444.0000263

Skamarock, W. C., Klemp, J. B., Dudhia, J., Gill, D. O., Liu, Z., Berner, J., et al. (2019). *A description of the advanced research WRF model version 4* (Vol. 145). National Center for Atmospheric Research.

Slater, A., Bohn, T., McCreight, J., Serreze, M., & Lettenmaier, D. (2007). A multimodel simulation of pan-arctic hydrology. *Journal of Geophysical Research*, *112*(G4), ARTN G04S45. https://doi.org/10.1029/2006jg000303

Steadman, R. G. (1979). The assessment of sultriness. Part I: A temperature-humidity index based on human physiology and clothing science. *Journal of Applied Meteorology and Climatology*, *18*(7), 861–873. https://doi.org/10.1175/1520-0450(1979)018<0861:taospi>2.0.co;2

Stein, U., & Alpert, P. (1993). Factor separation in numerical simulations. *Journal of the Atmospheric Sciences*, *50*(14), 2107–2115. https://doi.org/10.1175/1520-0469(1993)050<2107:fsins>2.0.co;2

Stergiou, I., Tagaris, E., & Sotiropoulou, R. E. P. (2017). Sensitivity assessment of WRF parameterizations over Europe. In *Multidisciplinary digital* (Vol. 1, p. 119). Publishing Institute Proceedings. https://doi.org/10.3390/ecas2017-04138

Stewart, I. D., & Oke, T. R. (2012). Local climate zones for urban temperature studies. *Bulletin of the American Meteorological Society*, *93*(12), 1879–1900. https://doi.org/10.1175/bams-d-11-00019.1

Taylor, K. E. (2001). Summarizing multiple aspects of model performance in a single diagram. *Journal of Geophysical Research*, *106*(D7), 7183–7192. https://doi.org/10.1029/2000jd900719

Teuling, A. J., Seneviratne, S. I., Stöckli, R., Reichstein, M., Moors, E., Ciais, P., et al. (2010). Contrasting response of European forest and grassland energy exchange to heatwaves. *Nature Geoscience*, *3*(10), 722–727. https://doi.org/10.1038/ngeo950

Varentsov, M., Samsonov, T., & Demuzere, M. (2020). Impact of urban canopy parameters on a megacity's modelled thermal environment. *Atmosphere*, *11*(12). https://doi.org/10.3390/atmos11121349

World Bank, T. (2021). *Urban population (% of total population)-European Union*. Retrieved from https://data.worldbank.org/indicator/SP.URB.TOTL.ZS?locations=Eu

Xu, X., Chen, F., Shen, S., Miao, S., Barlage, M., Guo, W., & Mahalov, A. (2018). Using WRF-urban to assess summertime air conditioning electric loads and their impacts on urban weather in Beijing. *Journal of Geophysical Research: Atmospheres*, *123*(5), 2475–2490. https://doi.org/10.1002/2017jd028168

Yang, L., Smith, J., & Niyogi, D. (2019). Urban impacts on extreme monsoon rainfall and flooding in complex terrain. *Geophysical Research Letters*, *46*(11), 5918–5927. https://doi.org/10.1029/2019gl083363

Yang, Z. L., Niu, G. Y., Mitchell, K. E., Chen, F., Ek, M. B., Barlage, M., et al. (2011). The community NOAH land surface model with multiparameterization options (NOAH-MP): 2. Evaluation over global river basins. *Journal of Geophysical Research*, *116*(D12). https://doi.org/10.1029/2010jd015140

Zhao, L., Oleson, K., Bou-Zeid, E., Krayenhoff, E. S., Bray, A., Zhu, Q., et al. (2021). Global multi-model projections of local urban climates. *Nature Climate Change*, *11*(12), 1–6. https://doi.org/10.1038/s41558-020-00958-8

Zonato, A., Martilli, A., Di Sabatino, S., Zardi, D., & Giovannini, L. (2020). Evaluating the performance of a novel WUDAPT averaging technique to define urban morphology with mesoscale models. *Urban Climate*, *31*, 100584. https://doi.org/10.1016/j.uclim.2020.100584